2024 IEEE International Conference on Robotics and Automation (ICRA 2024)
May 13-17, 2024. Yokohama, Japan

Stiffness-Based Hybrid Motion/ Force Control for Cable-Driven Serpentine Manipulator*

Wenshuo Li, *Student Member*, *IEEE*, Wenfu Xu, *Senior Member*, *IEEE*, Peisheng Huang, Boyang Lin, Bin Liang, *Senior Member*, *IEEE*

***Abstract*— In recent years, there has been a growing demand for robotic manipulators to perform tasks in various unstructured environments and situations requiring precision and force control. However, traditional robotic arms have limitations in fully leveraging their advantages in such scenarios. To address this demand, we have designed a cable-driven serpentine manipulator (CDSM) that combines force and precision motion control. This control method allows for precise manipulation of forces and torques at the end-effector, particularly in applications like electric vehicle charging and narrow-space exploration. It also enables independent control in multiple configurations. We achieve force-position hybrid control in task space, ensuring accurate control of end-effector force while achieving precise position control in other directions. Additionally, we implement joint angle closed-loop control in joint space to reduce the impact of cable elasticity deformation and friction on joint motion accuracy. Finally, servo control is applied at the lowest motor level. This paper investigates the modeling, sensing, and control of CDSM within a unified framework of hybrid motion/force control. Through experiments and simulations, we demonstrate the high accuracy and practicality of this control method in various scenarios.**

Keywords: Cable-driven serpentine manipulator; Stiffness modeling; Hybrid motion/ force control;

I. Introduction

Cable-driven serpentine manipulator (CDSM), inspired by the biomechanics of animals, offer unique advantages including slender and continuous body structures, inherent compliance, and flexible motion capabilities [1]. These distinctive features empower cable-driven manipulators to excel in constrained and narrow operating spaces [2], [3]. The literature showcases a wide array of practical applications, spanning from minimally invasive surgery [4], [5] and the manipulation of toxic chemicals and nuclear waste [6], [7] to search and rescue missions and inspections in space and other challenging environments [8].

In the realm of industrial automation and artificial intelligence, the widespread adoption of the force-position hybrid control mode in various robotic applications has gained significant traction[9], [10], [11]. This mode, notably effective in intricate operations such as fine assembly and robotic surgery, is characterized by its remarkable flexibility and precision.

Traditionally, research on hybrid control at the end-effector of collaborative robotic arms has matured considerably [12]. Typically, in these scenarios, it involves computing the appropriate Jacobian matrix to transform force vectors at the end-effector into joint torques. This allows for direct torque control at the joints, enabling force-position hybrid control at the end-effector. However, the landscape changes with CDSM, as they are driven by cables not directly actuated at the joints but through cable-driven motion. In this context, establishing the relationship between the end-effector's force vectors and the cable tensions (or motor displacements in the case of positional control) becomes a complex challenge. This complexity arises due to the intricate multi-dimensional mapping between task space, joint space, cable space, and motor drive space that is inherent to CDSM.

One alternative approach to mapping force vectors at the end-effector to joint space displacements is the utilization of stiffness models. However, traditional stiffness models exhibit limited accuracy and control capabilities when applied to flexible mechanical arms, particularly those driven by cables. This limitation stems from the highly nonlinear and unmodeled dynamic behaviors exhibited by this class of robots.

In the field of stiffness analysis, many researchers have introduced the concept of different space stiffness due to the complexity and challenges associated with modeling [13]. Additionally, Yuan. et al. have proposed a numerical method for stiffness calculation based on the principle of virtual work and provided theoretical insights for deformation compensation [14]. Nevertheless, these methods have not been extensively applied to stiffness control in cable-driven manipulator.

In previous stages of our research [15], we explored aspects of admittance control to directly convert end-effector force vectors into joint space displacements, effectively addressing the limitation of not being able to apply direct joint torque control. However, for specific task scenarios requiring precise force control, the effectiveness of this approach often fell short of expectations.

To address these challenges comprehensively, this paper delves into the design and implementation of a stiffness-based force-position hybrid control mode tailored for CDSM. This novel control method combines closed-loop control in joint space with the tension constraint control in cable space, enabling a more accurate understanding of the dynamic

* This work was supported in part by the National Natural Science Foundation of China (Grant No. 92248304, 62203140), Program of Shenzhen Peacock Innovation Team (Grant No. KQTD20210811090146075), and the Basic Research Program of Shenzhen (JCYJ20220818102415034). (Corresponding authors: Bin Liang).

Bin Liang is with the Department of Automation, Tsinghua University, Beijing 100854, China (e-mail: bliang@tsinghua.edu.cn).

Wenshuo Li, Wenfu Xu, Peisheng Huang, and Boyang Lin are with the School of Mechanical Engineering and Automation, Harbin Institute of Technology, Shenzhen 518055, China. They are also with Guangdong Key Laboratory of Intelligent Morphing Mechanisms and Adaptive Robotics (e-mail: 20b953005@stu.hit.edu.cn; wfxu@hit.edu.cn; 21s153224@stu.hit.edu.cn; 22s153179@stu.hit.edu.cn).

behaviors of both the cables and the joints. Ultimately, this approach facilitates precise end-effector force-position hybrid control in the realm of cable-driven manipulators.

The remainder of this paper is structured as follows: In Section II, we provide a concise overview of the multiple mapping relations and the stiffness model within the CDSM system. Section III delves into a detailed explanation of the principles behind end-effector force-position hybrid control, elucidating the logical relationships that govern the entire control system. Following a brief overview of the electrical system, Section IV showcases the results typical experiment. Finally, we encapsulate the findings and contributions of this paper in Section V.

II. System Design And Modeling

A. Simple Kinematics and multi-mapping

The main body of the CDSM consists of N rigid links, N universal joints, and $3N$ driven cables. The links are serially connected through universal joints. The driven cables pass through holes in the links and discs, with one end fixed to the end disc (fixture) of the link and the other end fixed to a machine part. This side includes a tension sensor primarily used to measure cable tension. Each universal joint has two degrees of freedom (DOFs) and is independently driven by three cables, allowing for individual motion. The two rotation directions of a universal joint are defined as Pitch and Yaw.

Based on the symmetry of the mounting structure, the layout of N universal joints in the CDSM alternates between (Yaw - Pitch) and (Pitch - Yaw). Two fixed absolute magnetic angle encoders are integrated within each joint to measure the two angle values. The specific structural arrangement is shown in Fig. 1 (a) and (b).

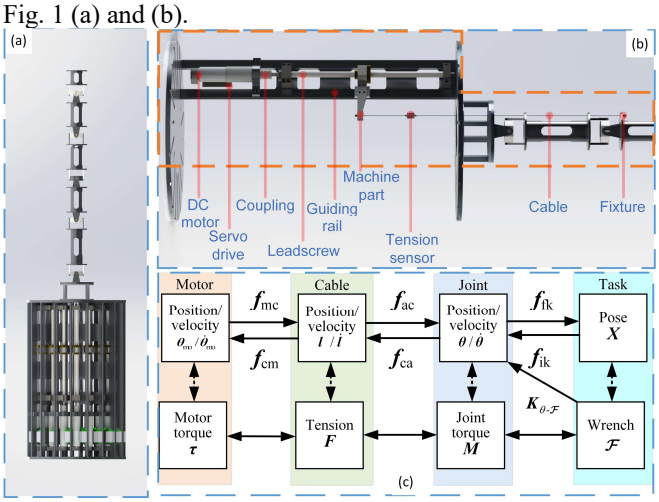

Fig. 1. Overview of the CDSM design. (a) Holistic structure. (b) Cut-away view of the modular driven unit. (c) Multi-space mapping.

According to design above, there exist multiple mapping relationship among $3N$ motors, $3N$ cables, N joints and end-effector ($\mathbb{R}^{6\times1}$). Hence, comprehensive kinematics between various spaces including corresponding states such as position, velocity, acceleration, force, and torque, need to be established, as depicted in Fig. 1 (c). The motor angles, cable lengths, joint angles, end-effector pose are respectively denoted as $\boldsymbol{\theta}_{\mathrm{mo}}$, $\boldsymbol{l}$, $\boldsymbol{\theta}$, and $\boldsymbol{X}$. Correspondingly, the motor torques, cables tensions, joint torques and end-effector wrench are denoted as $\boldsymbol{\tau}$, $\boldsymbol{F}$, $\boldsymbol{M}$, and $\boldsymbol{\mathcal{F}}$.

B. Stiffness modeling

In our previous work, our researches extensively elaborated on the calculations involving the motor-cable-joint forward and inverse kinematics (*FK& IK*) [1], [2], [16]. Furthermore, to achieve more precise force control, it is imperative to establish the relationship between end-effector $\boldsymbol{\mathcal{F}}$ and the joint variables, which is essentially a stiffness problem.

CDSM has $2N$ degrees and can only achieve rotational motions while lacking translational capabilities. This implies that we only need to consider angular displacements caused by wrench. To calculate stiffness, it is essential to establish the relationship between cable tensions and external torques. According to the principle of virtual work (PVW), the work performed by cable tension $\boldsymbol{F}$ is equivalent to the work executed by the joint torque $\boldsymbol{M}$ applied at the joints. In other words, these two quantities are equal, as expressed by the equation

$$\dot{\boldsymbol{l}}^T\boldsymbol{F}=\dot{\boldsymbol{\theta}}^T\boldsymbol{M} \tag{1}$$

The relationship between cable velocity $\dot{\boldsymbol{l}}$ and joint angular velocity $\dot{\boldsymbol{\theta}}$ can be obtained through differentiation as below

$$\dot{l}_i=\dot{\boldsymbol{\theta}}^T\begin{bmatrix}\dfrac{\partial l_i}{\partial\theta_1} & \cdots & \dfrac{\partial l_i}{\partial\theta_{2N}}\end{bmatrix}^T \tag{2}$$

Combining equations (1) and (2), the relationship between the equivalent joint torque and cable tension is analogous to the relationship between cable velocity and joint angular velocity, as follows

$$\boldsymbol{M}=\boldsymbol{J}_{l-\theta}^T\boldsymbol{F} \tag{3}$$

$$\dot{\boldsymbol{l}}=\boldsymbol{J}_{l-\theta}^T\dot{\boldsymbol{\theta}} \tag{4}$$

where $\boldsymbol{J}_{l\text{-}\theta}$ is a Jacobian matrix with $\mathbb{R}^{3N\times2N}$, which can be defined as:

$$\boldsymbol{J}_{l-\theta}^T=\begin{bmatrix}\dfrac{\partial l_1}{\partial\theta_1} & \dfrac{\partial l_2}{\partial\theta_1} & \cdots & \dfrac{\partial l_{3N}}{\partial\theta_1}\\ \dfrac{\partial l_1}{\partial\theta_2} & \dfrac{\partial l_2}{\partial\theta_2} & \cdots & \dfrac{\partial l_{3N}}{\partial\theta_2}\\ \vdots & \vdots & \vdots & \vdots\\ \dfrac{\partial l_1}{\partial\theta_{2N}} & \dfrac{\partial l_2}{\partial\theta_{2N}} & \cdots & \dfrac{\partial l_{3N}}{\partial\theta_{2N}}\end{bmatrix}^T \tag{5}$$

According to equation (3), we can obtain the variation $\delta\boldsymbol{M}$ as follows

$$\delta\boldsymbol{M}=\delta\boldsymbol{J}_{l-\theta}^T\boldsymbol{F}+\boldsymbol{J}_{l-\theta}^T\delta\boldsymbol{F} \tag{6}$$

It's worth noting that the tension in the cable is proportional to its deformation as $F_i=k\delta l_i$, and the cable stiffness k is related to its initial length. Define the joint-space stiffness matrix $\boldsymbol{K}_\theta$ for the CDSM as $\delta\boldsymbol{M}=\boldsymbol{K}_\theta\delta\boldsymbol{\theta}$. Substituting the definitions of $\boldsymbol{K}_\theta$ and cable stiffness k into equation (4) and combining it with equation (6), we can obtain

$$\boldsymbol{K}_\theta\delta\boldsymbol{\theta}=\delta\boldsymbol{J}_{l-\theta}^T\boldsymbol{F}+k\boldsymbol{J}_{l-\theta}^T\delta\boldsymbol{l}=\delta\boldsymbol{J}_{l-\theta}^T\boldsymbol{F}+k\boldsymbol{J}_{l-\theta}^T\boldsymbol{J}_{l-\theta}\delta\boldsymbol{\theta} \tag{7}$$

As a result, we can obtain the joint stiffness matrix of the CDSM as follows:

$$\boldsymbol{K}_{\theta}=\frac{\delta \boldsymbol{J}_{l-\theta}^{T}}{\delta \boldsymbol{\theta}} \boldsymbol{F}+k \boldsymbol{J}_{l-\theta}^{T} \boldsymbol{J}_{l-\theta} \tag{8}$$

Furthermore, the $\frac{\delta \boldsymbol{J}_{l-\theta}^{T}}{\delta \boldsymbol{\theta}}$ in equation (8) can be further expressed as

$$\begin{aligned}
\frac{\delta \boldsymbol{J}_{l-\theta}^{T}}{\delta \boldsymbol{\theta}} &= \sum_{i=1}^{3N} \frac{\delta \boldsymbol{J}_{i}}{\delta \boldsymbol{\theta}} \boldsymbol{F}=\frac{\delta\left[\boldsymbol{J}_{1} \quad \boldsymbol{J}_{2} \quad \cdots \quad \boldsymbol{J}_{3N}\right] \boldsymbol{F}}{\delta \boldsymbol{\theta}} \\
&=\left[\begin{array}{cccc} \frac{\delta \boldsymbol{J}_{1}}{\delta \boldsymbol{\theta}} & \frac{\delta \boldsymbol{J}_{2}}{\delta \boldsymbol{\theta}} & \cdots & \frac{\delta \boldsymbol{J}_{3N}}{\delta \boldsymbol{\theta}} \end{array}\right] \boldsymbol{F} \\
&=\sum_{i=1}^{3N}\left[\begin{array}{cccc} \frac{\partial^{2} l_{i}}{\partial \theta_{1}^{2}} & \frac{\partial^{2} l_{i}}{\partial \theta_{1} \partial \theta_{2}} & \cdots & \frac{\partial^{2} l_{i}}{\partial \theta_{1} \partial \theta_{2N}} \\ \frac{\partial^{2} l_{i}}{\partial \theta_{2} \partial \theta_{1}} & \frac{\partial^{2} l_{i}}{\partial \theta_{2}^{2}} & \cdots & \frac{\partial^{2} l_{i}}{\partial \theta_{2} \partial \theta_{2N}} \\ \vdots & \vdots & \vdots & \vdots \\ \frac{\partial^{2} l_{i}}{\partial \theta_{2N} \partial \theta_{1}} & \frac{\partial^{2} l_{i}}{\partial \theta_{2N} \partial \theta_{2}} & \cdots & \frac{\partial^{2} l_{i}}{\partial \theta_{2N} \partial \theta_{2N}} \end{array}\right] F_{i} \\
&=\sum_{i=1}^{3N} \mathbf{H}(l_{i}) F_{i}
\end{aligned} \tag{9}$$

where $\mathbf{H}(l_i)$ represents the Hessian matrix of i-th cable. Therefore, the stiffness matrix $\boldsymbol{K}_{\theta}$ of the manipulator can be further written as:

$$\boldsymbol{K}_{\theta}=\sum_{i=1}^{3N} F_{i} \mathbf{H}(l_{i})+k \boldsymbol{J}_{l-\theta}^{T} \boldsymbol{J}_{l-\theta} \tag{10}$$

In order to calculate the stiffness matrix $\boldsymbol{K}_{\theta}$, it is necessary to provide the current cable tensions $\boldsymbol{F}$ and joint angles $\boldsymbol{\theta}$. Since all joints of the CDSM are actively driven and are in a load-free static equilibrium when the external torque applied to the joints is zero, this implies that equation (3) can be written as:

$$\mathbf{0}=\boldsymbol{J}_{l-\theta}^{T} \boldsymbol{F} \tag{11}$$

In Equation (11), all solutions regarding the tensions $\boldsymbol{F}$ exist within the null space of $\boldsymbol{J}_{l-\theta}^{T}$. Additionally, with respect to the cable tensions, the constraint condition must also be satisfied, respectively:

Constraint 1: The tension values of each cable need to satisfy the preset minimum tension value $F_{\min}$. This ensures compliance with the minimum force threshold for low-level tension-joint control. Additionally, cables can withstand a maximum tension up to the breaking limit, denoted as $F_{\max}$.

$$F_{\min} \leq F \leq F_{\max} \tag{12}$$

In the process of end-effector force control, it is necessary to establish a relationship between the wrench $\boldsymbol{\mathcal{F}}$ and the joint angles. Therefore, by combining the above equations, we can obtain

$$\delta \boldsymbol{\theta}=\boldsymbol{K}_{\theta\text{-}\mathcal{F}} \delta \boldsymbol{\mathcal{F}}=\boldsymbol{K}_{\theta}^{-1} \boldsymbol{J}_{\mathrm{X}}^{\mathrm{T}} \delta \boldsymbol{\mathcal{F}} \tag{13}$$

Indeed, this also takes into consideration that CDSMs cannot directly control torque in joint-space. Therefore, the end-effector force is converted into changes in joint angles.

III. Hybrid Motion/Force control

In robotic force control, the dynamic characteristics of a robotic arm translate motion commands into actuator torque commands. Using this approach, the output units of both the force and motion controllers are consistent (typically torque). However, in the case of CDSM systems, there is no direct way to drive joint torques for individual joints. This is mainly due to the significant influence of multiple cables acting on each joint, leading to substantial coupling effects. Additionally, predicting frictional forces is more challenging, directly affecting the calculation precision of torque control. Another reason is that the dynamic modeling of CDSM is complex and high-cost computing, resulting in generally poor performance characteristics. Therefore, we propose to project wrench control commands into the motion controller under the joint space. Estimations of the robot allow maintaining unit consistency between the motion and force control branches.

Considering the requirements, this section addresses the design of a force/position hybrid controller and provides a brief explanation of the lower-level control logic involving joints, cables, and motors.

A. Task-space hybrid motion/force control

Before establishing the controller, the end-effector pose (position and orientation) $\boldsymbol{X}$ and the wrench $\boldsymbol{\mathcal{F}}$ are represented as follows

$$\begin{cases} \boldsymbol{X}=\begin{bmatrix} x & y & z & \alpha & \beta & \gamma \end{bmatrix}^{\mathrm{T}} \\ \boldsymbol{\mathcal{F}}=\begin{bmatrix} F_x & F_y & F_z & \tau_x & \tau_y & \tau_z \end{bmatrix}^{\mathrm{T}} \end{cases} \tag{14}$$

Due to the force and motion are controlled separately and independently of each other, we can write an equation called the reciprocity condition between them as:

$$\boldsymbol{X}^{\mathrm{T}} \boldsymbol{\mathcal{F}}=0 \tag{15}$$

The desired control torque should be a linear combination with one column of the matrix and related to the velocity. We can also define the force selective matrix $\boldsymbol{P}$ and motion selective matrix $\overline{\boldsymbol{P}}$ as follow:

$$\boldsymbol{P}=\begin{bmatrix} P_1 & & & \\ & P_2 & & \\ & & \ddots & \\ & & & P_6 \end{bmatrix}, \quad \overline{\boldsymbol{P}}=\boldsymbol{I}\text{-}\boldsymbol{P} \tag{16}$$

where $\boldsymbol{I}$ is the unit matrix, and the element P_m in $\boldsymbol{P}$ represents whether the m-th direction is selected for force control, in which case it is set to 1, and the corresponding direction is not controlled for motion. Once we obtain the end-effector wrench $\boldsymbol{\mathcal{F}}$, we can calculate the increment of the end-effector wrench through a PD controller as shown below:

$$\Delta \boldsymbol{\mathcal{F}}(t)=\boldsymbol{\mathcal{F}}_{\mathrm{d}}(t)+K_{\mathrm{P,F}} \boldsymbol{\mathcal{F}}_{\mathrm{e}}(t)+K_{\mathrm{D,F}} \frac{d \boldsymbol{\mathcal{F}}_{\mathrm{e}}(t)}{dt} \tag{17}$$

where $\boldsymbol{\mathcal{F}}_{\mathrm{e}}$ represents the error in the wrench vector, $\boldsymbol{\mathcal{F}}_{\mathrm{d}}$ is the desired force, and $\Delta\boldsymbol{\mathcal{F}}$(t) is the increment computed by the PD controller.

Next, we proceed with the calculation of the end-effector position. Given that we will perform individual control at the joint level, the error in the end-effector position can be obtained by numerically solving for the desired joint angles using the desired position $\boldsymbol{X}_{\mathrm{d}}$ and the current joint angle $\boldsymbol{\theta}_{\mathrm{cur}}$. This is expressed as follows:

$$\begin{cases} \boldsymbol{\theta}_{\mathrm{X,d}} = IK\left(\boldsymbol{X}_{\mathrm{d}}(t), \boldsymbol{\theta}_{\mathrm{cur}}(t)\right) \\ \Delta\boldsymbol{\theta}_{\mathrm{x}} = \boldsymbol{\theta}_{\mathrm{X,d}}(t) - \boldsymbol{\theta}_{\mathrm{cur}}(t) \end{cases} \tag{18}$$

where IK represents the inverse kinematics algorithm from the end-effector to the joint level. Finally, by merging the force/position control at the end-effector, we can summarize it as follows:

$$\Delta\boldsymbol{\theta}_{\mathrm{F/M}} = \boldsymbol{K}_{\theta\text{-}\mathcal{F}} \Delta\boldsymbol{\mathcal{F}}(t) + \Delta\boldsymbol{\theta}_{\mathrm{x}} \tag{19}$$

The above calculation yields the joint angle increments for the motion/force hybrid controller, and the task-space is gradually realized according to the low-level controller as shown in Fig. 2. When external F/T sensors are not available, the approach for end-effector force sensing can be referred to in [15].

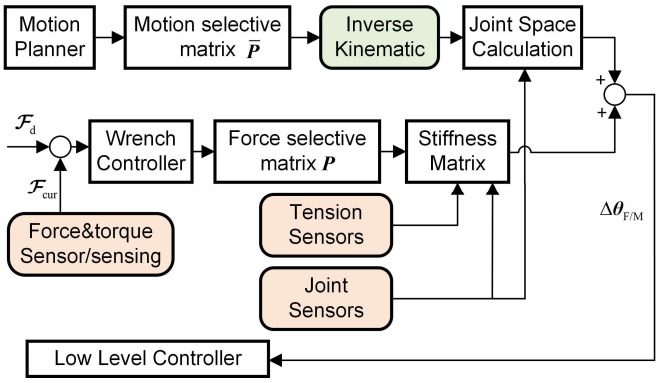

Fig. 2. Block diagram for a hybrid motion/force controller using F/T sensor (force sensing).

B. Low level controller

The lower-level controller comprises closed-loop control of joint angles, the velocity of cable, and the motor servo control. In practice, feedforward compensation control results in position errors accumulating over time. So, we adapt the PID controller in the joint-level, which has simple logical, strong robustness and excellent performance in control systems [43]. The controller can start the motion with the input of the desired trajectory angular velocity $\dot{\boldsymbol{\theta}}_{\mathrm{d}}$ and angle $\boldsymbol{\theta}_{\mathrm{d}}$ as feedforward, thus reducing error accumulation. The upper angle closed-loop control law is given by

$$\Delta\boldsymbol{\theta}(t) = \boldsymbol{\theta}_{\mathrm{d}}(t) + K_{\mathrm{P,a}}\boldsymbol{\theta}_{\mathrm{e}}(t) + K_{\mathrm{I,a}}\int_0^t \boldsymbol{\theta}_{\mathrm{e}}(t)dt + K_{\mathrm{D,a}}\frac{d\boldsymbol{\theta}_{\mathrm{e}}(t)}{dt} \tag{20}$$

where $\boldsymbol{\theta}_{\mathrm{d}}=\Delta\boldsymbol{\theta}_{\mathrm{F/M}}+\boldsymbol{\theta}_{\mathrm{X,d}}$ is the desired angles and $\boldsymbol{\theta}_{\mathrm{e}}=\boldsymbol{\theta}_{\mathrm{d}} - \boldsymbol{\theta}_{\mathrm{cur}}$ is the angular error signal of the single group. This controller combines the advantages of feedforward and feedback control. There is also a mapping between joint velocity and cable velocity of CDSM. A single universal joint has two DOFs, and each DOF requires a controller that outputs joint velocity instructions.

There is also a mapping between joint velocity and cable velocity of CDSM. A single universal joint has two DOFs, and each DOF requires a controller that outputs joint velocity command. The relationship between the motor speed $\dot{\boldsymbol{\theta}}_{\mathrm{mo}}$ and the cable speed $\tilde{\boldsymbol{l}}_{\mathrm{d}}$ is as follows

$$\dot{\boldsymbol{\theta}}_{\mathrm{mo}} = \boldsymbol{f}_{\mathrm{cm}}(\tilde{\boldsymbol{l}}_d) = \frac{c_{\mathrm{g}}\tilde{\boldsymbol{l}}_d}{S_{\mathrm{scr}}} \tag{21}$$

where c_g is the reduction ratio of gearbox and S_{scr} is ball screw lead. As a result of coupling effects, the absolute speed of the cable is superimposed on the other joints, and as follows

$$\dot{\boldsymbol{l}}_{\mathrm{d}} = \sum_{n=1}^{2N} \boldsymbol{f}_{\mathrm{ca}}(\boldsymbol{\theta}_n, \dot{\boldsymbol{\theta}}_n) \tag{22}$$

In the end, the movement of the CDSM is achieved by motor drivers and DC motors.

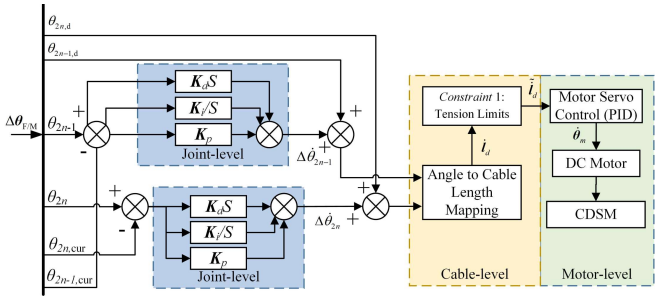

Fig. 3. Block diagram for the low level controller.

IV. Simulation and Experiment Analysis

A. Experimental setup

The hardware system primarily manages motor control, trajectory planning, control mode switching, and real-time status display of the CDSM [17]. This system comprises 15 DC motors and servo drives (Maxon®/Elmo®), necessitating the coordination of position and velocity control for all motors to meet their specific requirements. The joint encoder, tension sensor power amplifier signal lines, and the power supply unit are interconnected with the PCB, which, in turn, interfaces with the host computer via a serial port as shown in Fig. 4.

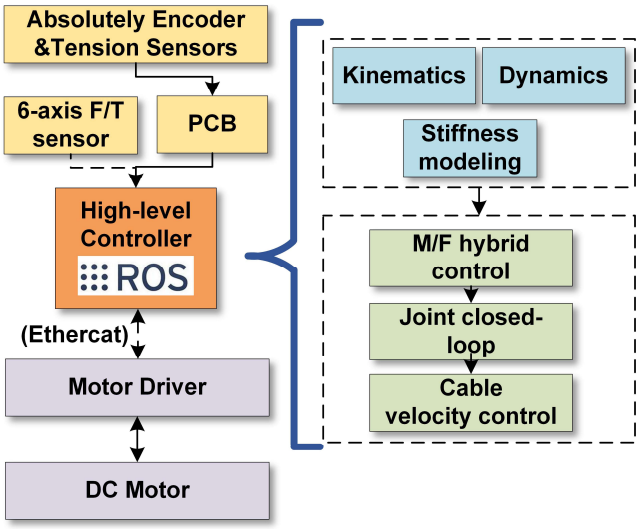

Fig. 4. The hardware system based on the ROS.

The hardware components are predominantly programmed in C++. Utilizing ROS Kinetic facilitates communication across different programming languages.

Regarding PID and PD controllers tuning, it's essential to perform tuning incrementally, starting from the lower layers and proceeding to the higher layers. This gradual approach ensures the robustness and rapid response of the controllers in each space. The controller parameters for the entire control

system, along with some basic parameters, are summarized in Table I.

Table I.
CONTROLLER PARAMETERS OF THE PROTOTYPE

Symbol	Property	Value
k	The cable stiffness	1e6N/m
$F_{\min}$	The minimum tension of cable	20N
$F_{\max}$	The maximum tension of cable	500N
$K_{P,F}$	Proportional coefficient of wrench control	4
$K_{D,F}$	Derivative coefficient of wrench control	2
$K_{P,a}$	Proportional coefficient of joint control	30
$K_{I,a}$	Integral coefficient of joint control	0.05
$K_{D,a}$	Derivative coefficient of joint control	0.1

Considering the structural characteristics and singularity issues of CDSM, the PD parameters for force/torque control along the x-axis can be adjusted to 1/2 to enhance system stability.

B. Experiment verification

To begin with, it is imperative to validate the performance of the hybrid motion/force controller. We have devised an experimental scenario in which the CDSM engages in a constant force linear motion on a flat surface, simulating a stain wiping experiment. The specific trajectory of the CDSM's vertical motion is depicted in Fig. 5.

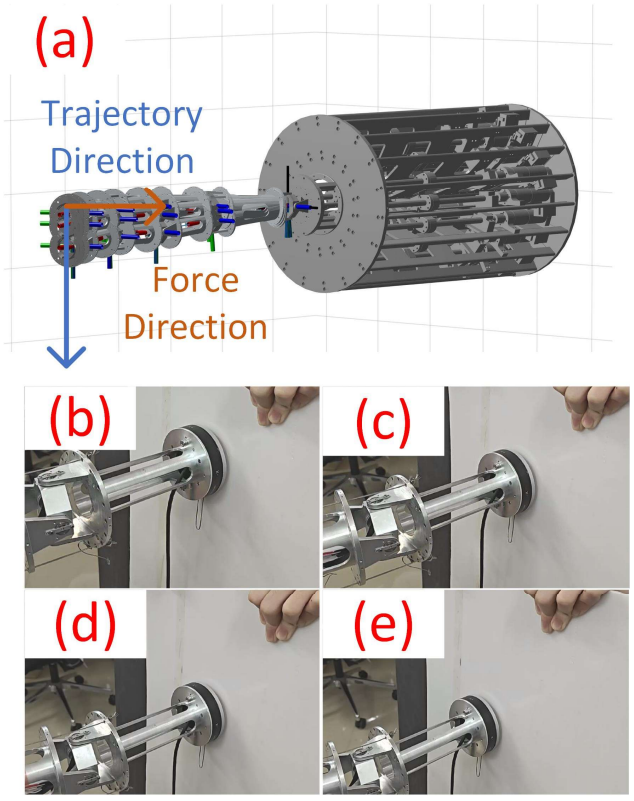

Fig. 5 (a) Diagram of the CDSM model built in MATLAB and labeled with force and trajectory directions. (b) – (e) Realistic Experimental Scenarios.

The entire motion execution can be divided into three distinct phases: pure position closed-loop control, force adjustment phase, and constant force control phase.

We initiated the experiment by utilizing position closed-loop control to move the system from an initial joint configuration, where all joint angles were set to 0, to a predefined initial configuration {0, 10, 10, 0, 0, 10, 10, 0, 5, 10}. Subsequently, within the ROS framework, we switched the control mode to the end-effector constant force control mode with an expected force of 3N. During the initial transition, the end-effector moved forward since it had no contact with the wiping surface, in accordance with the desired force. The contact phase involved a transition from zero to the desired force, as illustrated by the blue dashed box in Fig. 6. At this point, we executed a pre-planned linear trajectory to achieve the desired motion. Throughout the entire motion, the force's Mean Squared Error (MSE) and Root Mean Absolute Error (RMAE) were calculated as 0.391N and 0.556N, respectively, demonstrating the CDSM's notable force tracking capability.

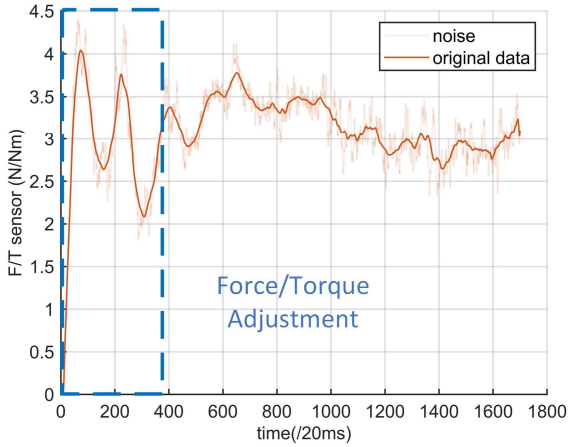

Fig. 6 The Actual force values by the F/T sensor, and the desired force is 3N.

On the other hand, an analysis from both the joint angle and position perspectives is presented in Fig. 7. The maximum angular error is found to be 1.33°, with the largest error occurring during the force/torque adjustment phase. The MAE for angles throughout the entire process is calculated as 0.239°.

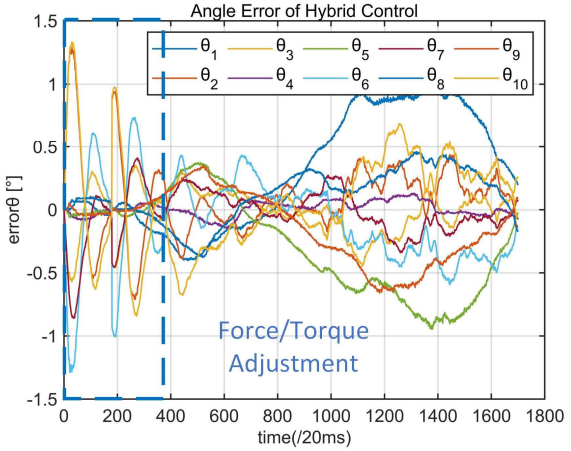

Fig. 7 The angle error of ten universal joints.

As shown in the Fig. 8, the position planning involves a linear motion segment, resulting in position MAE and RMSE values of 4.46 mm and 5.68 mm, respectively. This demonstrates that the flexible arm maintains a high level of overall motion accuracy while meeting the requirements of force control.

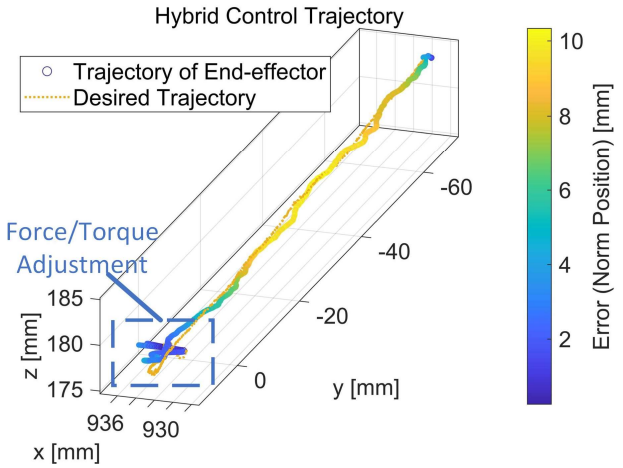

Fig. 8 Desired/ actual three-dimensional trajectory, and the color-bar shows the error of position.

For the purpose of achieving the minimum tension constraint in the cable space (*Constraint* 1), we devised a straightforward control approach to enforce constant minimal tension control, ensuring that min-tension cable maintain a minimum tension of 20 N, as shown in Table I and depicted in Fig. 9. Throughout the overall motion process described above, the cables are kept taut to impart a certain degree of stiffness to the flexible arm's overall structure.

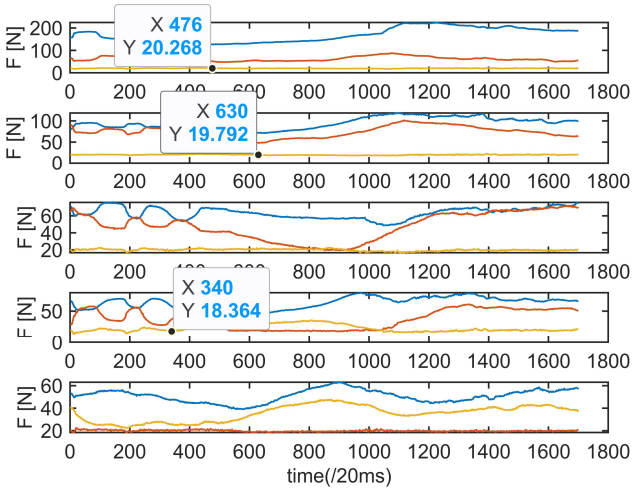

Fig. 9 The cable tension value based on the cable constraint conditions.

V. Conclusion

The paper primarily focuses on a CDSM designed to address the limitations of traditional robotic arms, such as their lack of precision and force control in intricate situations. Hence, we introduce a new alternative, a stiffness-based force-position hybrid control mode, tailored specifically for CDSM. This method synthesizes closed-loop control in joint space with the tension constraint in cable space, thereby enhancing the understanding of dynamic behaviors of both cables and joints. Accordingly, it enables precise end-effector force-position hybrid control within CDSM. Experimental results from the research have demonstrated positional accuracy reaching 4.46 mm and force accuracy of 0.39 N, underscoring the potential for CDSMs to expand their utility across a broader spectrum of applications.

Our forthcoming research endeavors will encompass tasks involving the redundant degrees of freedom in CDSMs, focusing on the rapid design and resolution of redundancy-related tasks, adaptive stiffness control, and human-robot interaction enhancements.

References

[1] W. Xu, T. Liu, and Y. Li, "Kinematics, Dynamics, and Control of a Cable-Driven Hyper-Redundant Manipulator," *IEEE/ASME Trans. Mechatron.*, vol. 23, no. 4, pp. 1693–1704, Aug. 2018.

[2] T. Liu, W. Xu, T. Yang, and Y. Li, "A Hybrid Active and Passive Cable-Driven Segmented Redundant Manipulator: Design, Kinematics, and Planning," *IEEE/ASME Trans. Mechatron.*, vol. 26, no. 2, pp. 930–942, Apr. 2021.

[3] M. T. Chikhaoui, S. Lilge, S. Kleinschmidt, and J. Burgner-Kahrs, "Comparison of Modeling Approaches for a Tendon Actuated Continuum Robot with Three Extensible Segments," *IEEE Robot. Autom. Lett.*, vol. 4, no. 2, pp. 989–996, Apr. 2019.

[4] J. Burgner-Kahrs, D. C. Rucker, and H. Choset, "Continuum Robots for Medical Applications: A Survey," *IEEE Trans. Robot.*, vol. 31, no. 6, pp. 1261–1280, 2015.

[5] W. Hong, L. Xie, J. Liu, Y. Sun, K. Li, and H. Wang, "Development of a Novel Continuum Robotic System for Maxillary Sinus Surgery," *IEEE/ASME Trans. Mechatron.*, vol. 23, no. 3, pp. 1226–1237, Jun. 2018.

[6] R. Buckingham and A. Graham, "Nuclear snake-arm robots," *Ind. Robot*, vol. 39, no. 1, pp. 6–11, 2012.

[7] J. Li and J. Xiao, "Progressive Planning of Continuum Grasping in Cluttered Space," *IEEE Trans. Robot.*, vol. 32, no. 3, pp. 707–716, Jun. 2016.

[8] H. Tsukagoshi, A. Kitagawa, and M. Segawa, "Active Hose: an artificial elephant's nose with maneuverability for rescue operation," in *Proc. IEEE Int. Conf. Robot. Autom. (ICRA)*, Seoul, Korea: IEEE, 2001, pp. 2454–2459 vol.3.

[9] A. Bajo and N. Simaan, "Hybrid motion/force control of multi-backbone continuum robots," *Int. J. Rob. Res.*, vol. 35, no. 4, pp. 422–434, Apr. 2016.

[10] K. Bai, W. Chen, K.-M. Lee, Z. Que, and R. Huang, "Spherical Wrist With Hybrid Motion-Impedance Control for Enhanced Robotic Manipulations," *IEEE Trans. Robot.*, vol. 38, no. 2, pp. 1174–1185, Apr. 2022.

[11] R. Yasin and N. Simaan, "Joint-level force sensing for indirect hybrid force/position control of continuum robots with friction," *Int. J. Rob. Res.*, vol. 40, no. 4–5, pp. 764–781, Apr. 2021.

[12] W. Gueaieb, F. Karray, and S. Al-Sharhan, "A Robust Hybrid Intelligent Position/Force Control Scheme for Cooperative Manipulators," *IEEE/ASME Trans. Mechatron.*, vol. 12, no. 2, pp. 109–125, Apr. 2007.

[13] L. Zhang, Y. Gao, Z. Mu, L. Yan, Z. Li, and M. Gao, "A Variable-Stiffness Planning Method Considering Both the Overall Configuration and Cable Tension for Hyper-Redundant Manipulators," *IEEE/ASME Trans. Mechatron.*, pp. 1–9, 2023.

[14] H. Yuan, W. Zhang, Y. Dai, and W. Xu, "Analytical and numerical methods for the stiffness modeling of cable-Driven serpentine manipulators," *Mech. Mach. Theory*, vol. 156, p. 104179, Feb. 2021.

[15] W. Li, X. Huang, L. Yan, H. Cheng, B. Liang, and W. Xu, "Force Sensing and Compliance Control for a Cable-Driven Redundant Manipulator," *IEEE/ASME Trans. Mechatron.*, vol. 29, no. 1, pp. 777–788, Feb. 2024.

[16] J. Peng, W. Xu, T. Yang, Z. Hu, and B. Liang, "Dynamic modeling and trajectory tracking control method of segmented linkage cable-driven hyper-redundant robot," *Nonlinear Dyn*, vol. 101, no. 1, pp. 233–253, Jul. 2020.

[17] W. Li, W. Xu, B. Lin, and L. Yan, "Design, Kinematics and Control of a Modular Cable-Driven Manipulator for Fine Manipulation," in *Proc. IEEE Int. Conf. Robot. Biomimetics. (ROBIO)*, Jinghong, China: IEEE, Dec. 2022, pp. 833–838.